A Library of Large-eddy Simulations for Calibrating Cloud Parameterizations

Zhaoyi Shen[1], Akshay Sridhar[1], Zhihong Tan[2], Anna Jaruga[1], Tapio Schneider[1,3]

[1]Department of Environmental Science and Engineering, California Institute of Technology, Pasadena, CA, USA
[2]Program in Atmospheric and Oceanic Science, Princeton University, Princeton, NJ, USA
[3]Jet Propulsion Laboratory, Pasadena, CA, USA

Key Points:

- A library of high-resolution simulations of clouds is created using LES driven by a GCM.
- The LES library can be used to train parameterizations in a GCM and to investigate cloud feedbacks.

Corresponding author: Zhaoyi Shen, zhaoyi@caltech.edu

Abstract

Advances in high-performance computing have enabled large-eddy simulations (LES) of turbulence, convection, and clouds, but their potential to improve parameterizations in global climate models (GCMs) is only beginning to be harnessed. We design an experimental setup in which LES can be driven by large-scale forcings from GCMs. This can be done anywhere in the atmosphere, and we use this setup to create a library of LES of clouds across tropical and subtropical regimes. The LES are used to simulate the transition from stratoculumus to shallow cumulus over the East Pacific. The results are not very sensitive to the choice of the host GCM driving the LES. The setup is also used to simulate clouds under climate change. The LES simulate a positive but weak shortwave cloud feedback. The LES library expands the datasets available for calibrating parameterizations in GCMs.

Plain Language Summary

Clouds remain one of the largest uncertainties in our understanding and predictions of climate change because it is challenging to represent their small-scale dynamics in climate models. High-resolution simulations can provide faithful simulations of clouds and turbulence in limited areas, which can be used to calibrate climate models. However, only a limited set of simulations has been used for calibration of climate models, with focus on a few specific locations. This study presents an experimental setup that allows the high-resolution simulations to be run anywhere on the globe, driven by output from climate models. The setup is used to create a library of high-resolution simulations of clouds across different tropical and subtropical low-cloud regimes in both current and warmer climates. The library expands the training data available for the calibration and development of climate models.

1 Introduction

Low clouds play an important role in Earth's energy budget, but they are poorly represented in global climate models (GCMs). Despite some improvements in recent decades, large biases remain in the clouds simulated by the current generation of GCMs. Most GCMs underestimate low cloud cover in the tropics and subtropics (Klein et al., 2013; Cesana & Waliser, 2016; Vignesh et al., 2020). The negative model bias can be as large as 50% in stratocumulus regions near the coast (Brient et al., 2019). In shallow cumulus regions, most GCMs overestimate the optical thickness of low clouds to achieve a reasonable global-mean energy balance despite the low bias in cloud cover. This is referred to as the "too few, too bright" problem (Nam et al., 2012). How low clouds respond to global warming is a key source of uncertainty in predictions of climate change. While the low cloud feedback is generally positive in GCMs, the magnitude of the feedback has a large intermodel spread and is strongly correlated with the equilibrium climate sensitivity (Bony & Dufresne, 2005; Bony et al., 2006; Schneider, Teixeira, et al., 2017; Zelinka et al., 2020).

It is challenging for GCMs to simulate low clouds because their resolution, which is on the order of 100 km in the horizontal, is too coarse to resolve the boundary layer turbulence and convection controlling the clouds. As a result, GCMs rely on parameterizations to represent these processes, and inadequacies in the parameterizations lead to biases in GCM-simulated clouds. However, large-eddy simulations (LES) can directly resolve cloud dynamics and provide high-fidelity simulations in limited areas. While global LES will not be feasible for decades, data from LES can be used to train and improve GCM parameterizations with data assimilation and machine learning approaches (Schneider, Lan, et al., 2017). So far, LES used for evaluating GCM parameterizations have typically been run at a few specific locations, usually associated with field campaigns (e.g. Siebesma et al., 2003; Stevens et al., 2005; Rauber et al., 2007). Idealized large-scale forc-

ing fields are often used in studies comparing LES with GCMs and/or single column models (Zhang et al., 2012, 2013). The potential of using LES to systematically inform GCM parameterizations has not yet been fully harnessed.

In Shen et al. (2020), we presented a framework in which LES are driven by large-scale forcings from GCMs. This study aims to use the framework to expand the dataset for training GCM parameterizations by generating a library of LES across a range of cloud regimes. We simulate low-cloud over the East Pacific using LES driven by large-scale forcings from comprehensive GCMs in both current and warmer climates. Section 2 describes the GCM and LES used in the study and key features of the forcing framework. Section 3 describes simulation characteristics in the LES and compares the LES with the GCMs. Section 4 summarizes the conclusions and discusses potential uses of the data presented in this study.

2 Methods

2.1 Experimental Setup

The large-scale forcing is derived from the cfSites output in the Coupled Model Intercomparison Project Phase 5 (CMIP5) archive. cfSites includes high-frequency output at different locations of instrumented sites and field campaigns, as well as a number of climate regimes where the inter-model spread of cloud feedbacks is large (Bony et al., 2011). In this study, we focus on low cloud (cloud top height lower than 3km) regions over the East Pacific (Figure 1). We use 5-year (2004-2008) averaged large-scale forcings in different months (January, April, July, and October) from the AMIP experiment, which is forced by observed sea surface temperatures (SSTs) and sea ice concentration. The time-averaged forcing does not have a diurnal cycle. To test the sensitivity of the results to the host model, we use large-scale forcings from two GCMs: HadGEM2-A and CNRM-CM5. We choose these two models as the tropical low-cloud reflection response to global warming in HadGEM2-A and CNRM-CM5 are at the higher and lower end of the range of CMIP5 models, respectively (Brient & Schneider, 2016). To explore how clouds change in a warmer climate, we run simulations with large-scale forcings from the AMIP4K experiment, where SSTs are increased uniformly by 4 K from the AMIP experiment.

The LES are performed using the Python Cloud Large-Eddy Simulation (PyCLES) code (Pressel et al., 2015). PyCLES solves the anelastic equations with specific entropy and total water specific humidity as prognostic thermodynamic variables and uses a third-order, three-stage strong stability preserving Runge-Kutta scheme (Shu & Osher, 1988). The performance of the model on standard test cases has been described in previous papers (Pressel et al., 2015; Tan et al., 2016; Pressel et al., 2017). The simulations are forced with prescribed SSTs from the GCM. Surface fluxes are calculated using a bulk scheme with drag coefficients obtained from Monin-Obukhov similarity theory (Byun, 1990). Radiative energy fluxes are calculated with the Rapid Radiative Transfer Model (RRTM) (Iacono et al., 2008). The top-of-atmosphere insolation and the insolation-weighted average of solar zenith angle are prescribed from the GCM. Cloud microphysical processes are represented using a one-moment warm-rain microphysics scheme based on Kessler (1995). Subgrid-scale turbulent fluxes are modelled using the Smagorinsky-Lilly closure (Lilly, 1962; Smagorinsky, 1963). We use a doubly periodic domain that is 6000 m wide in the horizontal and 4000 m tall in the vertical. The horizontal and vertical resolutions are 75 m and 20 m, respectively. The time step is dynamically adjusted to maintain the Courant number close to 0.7, and is on the order of 1 s. The simulations are initialized from the 5-year averaged GCM profiles and are run for 6 days. The results are averaged over the last day, when most simulations reach a quasi-steady state.

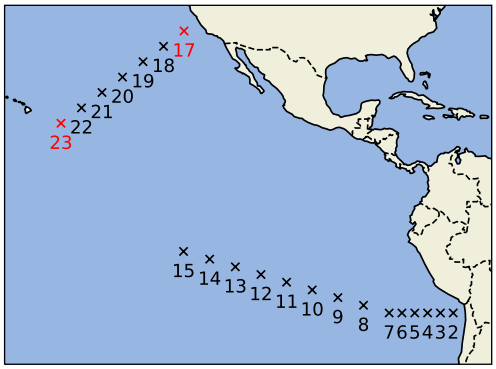

Figure 1: cfSites locations used in this study. The sites cover the transition from stratocumulus to shallow cumulus over the East Pacific. The red crosses highlight site 17 and site 23, two locations on which we focus in the paper. They represent cloud regimes of stratocumulus and shallow cumulus, respectively.

2.2 Forcing Framework

The forcing framework is similar to that in Shen et al. (2020). Here we briefly summarize the large-scale forcings in the LES and describe the difference to Shen et al. (2020).

2.2.1 Subsidence

Large-scale subsidence gives rise to a source in the specific entropy (s) and specific humidity (q_t) equations:

$$\frac{ds}{dt} = -\langle\tilde{w}\rangle\frac{\partial s}{\partial z}, \tag{1}$$

$$\frac{dq_t}{dt} = -\langle\tilde{w}\rangle\frac{\partial q_t}{\partial z}. \tag{2}$$

Here, $w = dz/dt$ is the vertical velocity, $\tilde{(\cdot)}$ denotes a GCM value, and $\langle\cdot\rangle$ denotes the time mean. The time-averaged vertical velocity is approximated by $\langle\tilde{w}\rangle \approx -\langle\tilde{\omega}\rangle\langle\tilde{\alpha}\rangle/g$, where we have ignored small terms associated with the horizontal advection of pressure and assumed that the pressure-coordinate vertical velocity $\tilde{\omega}$ and the specific volume $\tilde{\alpha}$ are uncorrelated.

2.2.2 Advection

Horizontal advection and vertical eddy advection are prescribed directly from the GCM as

$$\frac{ds}{dt} = \frac{c_p}{T}(\langle J_{\text{hadv}}\rangle + \langle J_{\text{veddy}}\rangle) + (s_v - s_d)(\langle S_{\text{hadv}}\rangle + \langle S_{\text{veddy}}\rangle), \tag{3}$$

$$\frac{dq_t}{dt} = \langle S_{\text{hadv}}\rangle + \langle S_{\text{veddy}}\rangle, \tag{4}$$

where c_p is the isobaric specific heat capacity of air; T is temperature; and s_d and s_v are specific entropies of dry air and water vapor, respectively. The terms S_{hadv} and J_{hadv} represent horizontal advection of specific humidity and temperature, and S_{veddy} and J_{veddy} represent vertical eddy advection of specific humidity and temperature. All four advection terms are derived from the GCM. The cfsites output includes total advective ten-

dencies of specific humidity ($S_{\rm adv}$) and temperature ($J_{\rm adv}$). We obtain the horizontal advective tendencies from the total advective tendencies as the residuals

$$S_{\rm hadv} = S_{\rm adv} + \tilde{w}\frac{\partial \tilde{q}_t}{\partial z}, \tag{5}$$

and

$$J_{\rm hadv} = J_{\rm adv} + \tilde{w}\frac{\partial \tilde{T}}{\partial z} + \tilde{w}\frac{g}{c_p}. \tag{6}$$

The vertical eddy advective tendencies are derived as

$$S_{\rm veddy} = -\left\langle \tilde{w}\frac{\partial \tilde{q}_t}{\partial z} \right\rangle + \langle \tilde{w} \rangle \frac{\partial \langle \tilde{q}_t \rangle}{\partial z}, \tag{7}$$

and

$$J_{\rm veddy} = -\left\langle \tilde{w}\frac{\partial T}{\partial z} \right\rangle + \langle \tilde{w} \rangle \frac{\partial \langle \tilde{T} \rangle}{\partial z}. \tag{8}$$

2.2.3 Relaxation

Unlike in Shen et al. (2020), the large-scale momentum forcing is not applied. Instead, the horizontal winds are relaxed to the GCM profiles on a timescale of 6 h. Free-tropospheric temperatures T and humidities q_t are relaxed to GCM profiles to prevent drifting from realistic conditions. The relaxation timescale varies with height as

$$\Gamma_r(z) = \frac{1}{\tau_r} \times \begin{cases} 0 & z < z_i, \\ 0.5\left(1 - \cos\left(\pi \frac{z - z_i}{z_r - z_i}\right)\right) & z_i \le z \le z_r, \\ 1 & z > z_r. \end{cases} \tag{9}$$

Relaxation forcing is commonly used when driving LES or single column models with GCMs or reanalysis, and the timescale is usually a few hours (e.g. Randall & Cripe, 1999; Neggers et al., 2012; Zhang et al., 2012). In this study, we set $\tau_r = 24$ h, and $z_r = 3500$ m and $z_i = 3000$ m.

3 Results

3.1 LES simulated low clouds

Figure 2 shows the cloud cover, cloud liquid water path (LWP), cloud base and cloud top at different sites in the LES driven by HadGEM2-A. The LES sample a wide range of cloud regimes. Near the coasts of Peru (sites 2–4) and California (sites 17–18), the simulations produce stratocumulus with cloud cover near 100%. The cloud cover decreases rapidly when moving away from the coast and is about 20–30% in shallow cumulus regions over the open ocean. The transition from stratocumulus to shallow cumulus is also seen in the decrease in LWP and the increase in cloud top height from the coast to the open ocean.

The cloud properties at different locations have distinct seasonal variations. In the stratocumulus regions off the coasts, cloud cover and LWP are higher in July and October in both hemispheres. In the shallow cumulus regions over the Southeast Pacific, cloud cover and LWP peak in July and show low values in January and April. The cloud base is highest in July and lowest in January, while the cloud top is generally higher in January than in July, suggesting some seasonal variation in the thickness of clouds. In the shallow cumulus regions over the Northeast Pacific, cloud cover and LWP show high values in April and low values in July. The cloud base is highest in April and lowest in July, and the seasonal variation in the cloud top generally follows that in the cloud base height.

The cloud properties in the LES driven by CNRM-CM5 are shown in Figure 3. Unlike the LES driven by HadGEM2-A, this LES does not simulate a stratus cloud layer near the coast of Peru. In the shallow cumulus regions, the cloud fraction and LWP in some seasons are higher than that in the LES driven by HadGEM2-A, which largely results from differences at the cloud top. The differences between the two host GCMs will be discussed further in Section 3.2.

Figures 4 and 5 show the vertical profiles of large-scale forcings and cloud properties of two sites over the Northeast Pacific in HadGEM2-A in July, representing the cloud regimes of stratocumulus (site 17) and shallow cumulus (site 23). The large-scale subsidence is stronger at site 17 than at site 23. There is horizontal advective cooling and drying in the boundary layer at both sites, and their tendencies are stronger at site 17. The advective tendencies are consistent with the lower-level winds, which are northerly near the coast (site 17) and northeasterly away from the coast (site 23).

Figure 6 shows the timeseries of cloud cover and LWP at sites 17 and 23. The LES reach quasi-steady states in 1–2 days at both sites, although the relatively small domain size leads to high-frequency oscillations especially for shallow cumulus. The LES simulate stratocumulus under strong subsidence and advective cooling and drying at site 17, with a cloud top at around 1000 m and a cloud fraction close to 100% (Figure 4g). The stratocumulus layer is slightly decoupled from the subcloud mixed layer, as seen in the vertical profiles of total water specific humidity, liquid potential temperature, and vertical velocity variance below the inversion (Figures 4d–4f). This decoupling may be due to the strong advective cooling at the bottom of the cloud layer (Figure 4b). At site 23, the LES simulates a shallow cumulus layer with a cloud base at around 500 m and a cloud top at around 1600 m. The cloud fraction and the corresponding vertical velocity variance have two peaks (Figures 5d and 5h): just above the lifted condensation level and just below the inversion. The anvil resulting from the detrainment of cumulus updrafts is ubiquitous in the LES simulations of shallow cumulus sites.

3.2 Comparison to GCM and sensitivity to large-scale forcing

We compare the LES-simulated cloud profiles with those in the host GCM, HadGEM2-A (Figures 4g, 4h, 5g, and 5h). At site 17 in July, the GCM produces a lower but deeper stratocumulus layer. The cloud base in the GCM is very close to the surface and lower than that in the LES by about 400 m, while the cloud top heights are similar between the GCM and the LES. The maximum cloud fraction and cloud liquid water in the GCM are much smaller than in the LES, and LWP in the GCM is about 40% smaller. At site 23, the GCM produces a higher and deeper shallow cumulus layer. The cloud base in the GCM is slightly lower than in the LES, while the cloud top in the GCM is about 500 m higher. The cloud fraction and cloud liquid water in the GCM are much larger. The GCM only produces one peak in cloud fraction in the middle of the shallow cumulus layer, as opposed to the two peaks at the bottom and the top of the cloud layer in the LES.

Figure 7a compares LWP at all sites simulated by HadGEM2-A and LES. The spread of LWP at different sites is much smaller in the LES than in the GCM, and there is no correlation between the LES and the GCM. In the shallow cumulus regions, LWP is systematically larger in the GCM, mostly resulting from a deeper cloud layer. The difference can be as large as 60 g m^{-2} at several sites (e.g., over the North Pacific). In the stratocumulus regions, the LWP differences between the GCM and the LES are smaller, although the maximum cloud fraction in the stratocumulus layer in the GCM is always much smaller than in the LES. This is because the cloud layer is usually much thicker in the GCM (e.g., Figures 4g and 4h).

The large-scale forcing used to drive the LES is dependent on the host GCM. Figure 8 shows the vertical profiles of large-scale forcings and cloud properties in the LES driven by the two GCMs, HadGEM2-A and CNRM-CM5, at sites 17 and 23 in July. At

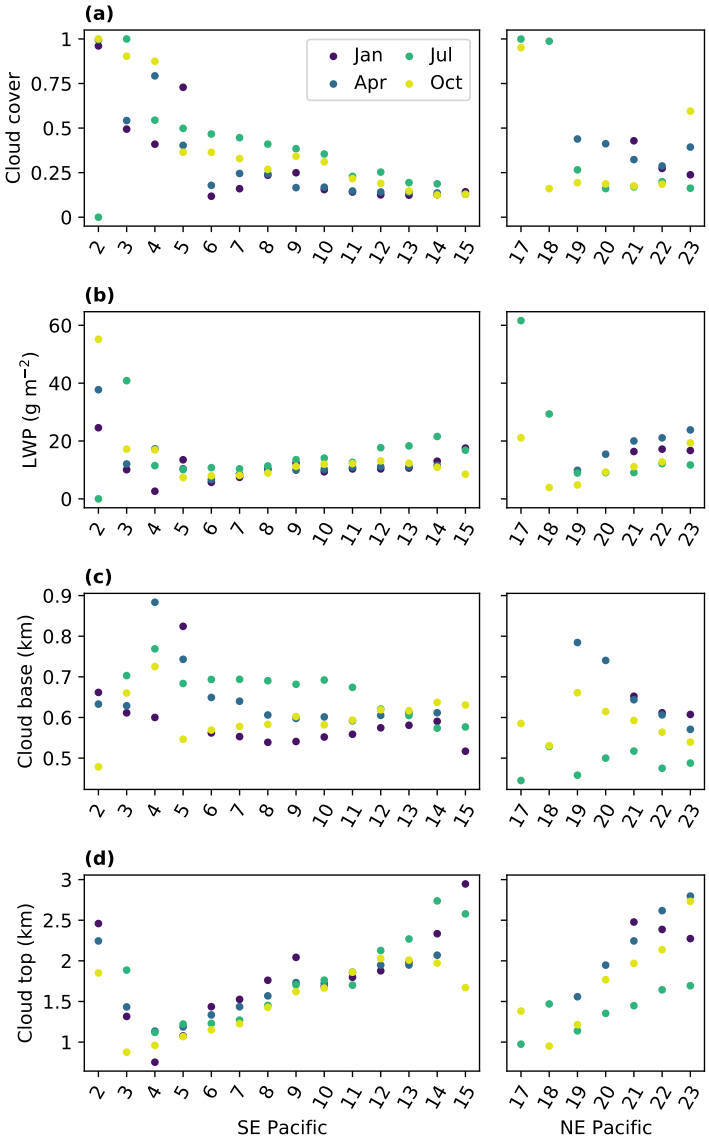

Figure 2: (a) Cloud cover, (b) cloud liquid water path (LWP), (c) cloud base height, and (d) cloud top height at different sites in the LES driven by HadGEM2-A in different seasons. Missing points indicate the cloud top height is higher than 3000 m.

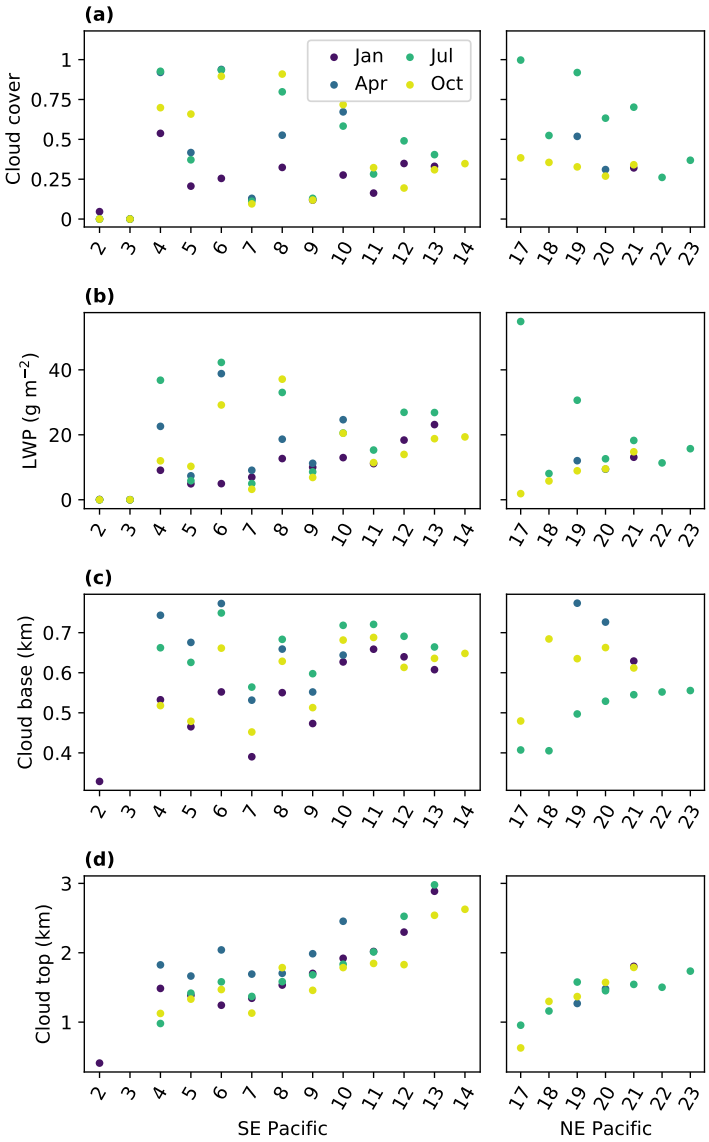

Figure 3: Same as Figure 2 but for LES driven by CNRM-CM5.

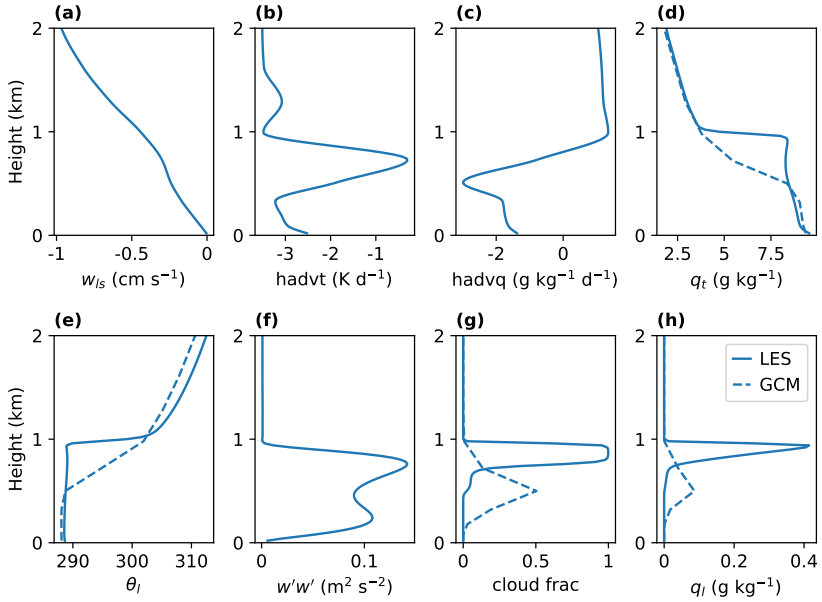

Figure 4: Vertical profiles of (a) large-scale vertical velocity, (b) horizontal advection of temperature, (c) horizontal advection of specific humidity, (d) total water specific humidity, (e) liquid potential temperature, (f) vertical velocity variance, (g) cloud fraction, and (h) cloud liquid water specific humidity in the LES driven by HadGEM2-A at site 17 in July. The dashed lines represent the GCM profiles.

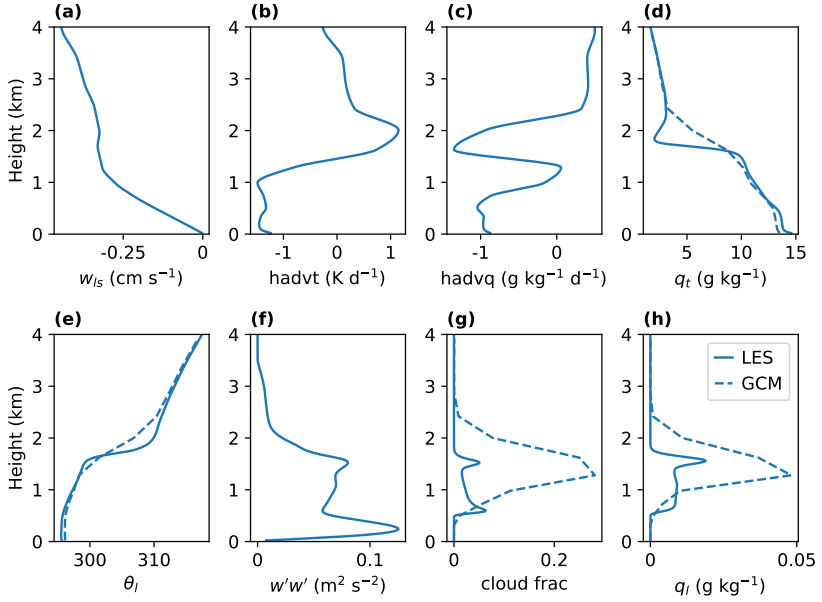

Figure 5: Same as Figure 4, but for site 23 in July.

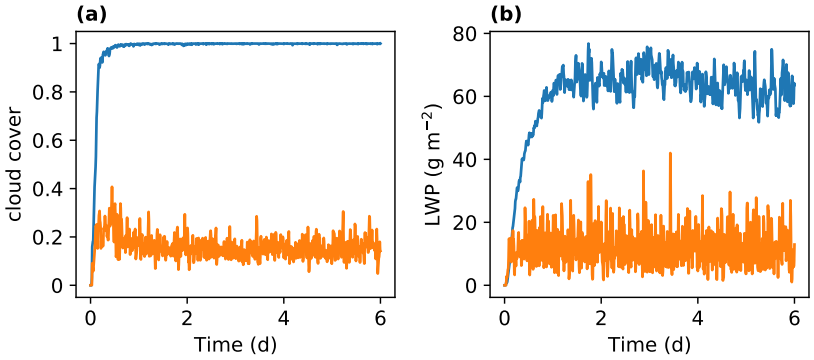

Figure 6: Time series of (a) cloud cover and (b) liquid water path in the LES driven by HadGEM2-A. Blue and orange lines represent sites 17 and 23 in July, respectively.

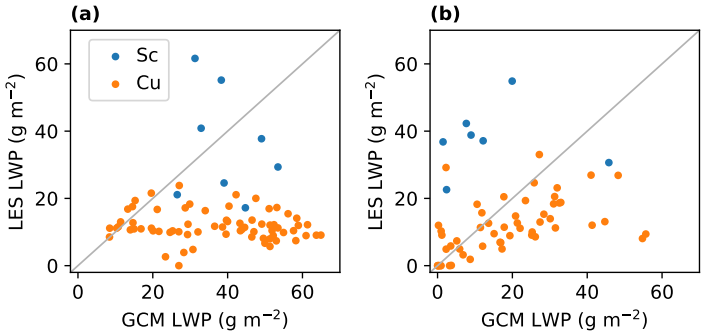

Figure 7: Scatter plot of LWP in the LES and GCM at different sites. Blue and orange dots represent stratocumulus (Sc) and shallow cumulus (Cu) in the LES, respectively. The host GCMs are (a) HadGEM2-A and (b) CNRM-CM5.

site 17, the subsidence and horizontal advection of temperature and moisture are generally similar between the two GCMs. The vertical profiles of cloud fraction and cloud liquid water in the LES driven by forcing from the two GCMs are almost identical. While there are some differences in the GCM-simulated cloud profiles, the cloud layers in both GCMs are thicker than that in the LES, and the maximum cloud fraction and cloud liquid water are smaller. The difference in the large-scale forcing at site 23 is larger. Compared to HadGEM2-A, CNRM-CM5 has a weaker subsidence and a stronger boundary layer cooling and drying. The LES driven by forcings from the two GCMs yields similar vertical profiles of shallow cumulus in general, except that the cloud fraction at the cloud top is larger in the LES driven by CNRM-CM5. However, the differences between the GCMs are much larger. Compared to HadGEM2-A, the shallow cumulus layer in CNRM-CM5 has a lower cloud top and much smaller cloud fraction and cloud liquid water.

Figure 9 compares the differences in the GCM- and LES-simulated LWP at all sites in different seasons. The magnitudes of the differences between the LES are smaller than 15 g m^{-2} for most cases. The difference between the GCMs are much larger. In general, LWP in CNRM-CM5 is smaller than in HadGEM2-A, and the magnitudes of the differences are as large as 40 to 50 g m^{-2} at several sites. The magnitudes of the differences averaged over all cases in the LES and the GCMs are 0.5 and 23.9 g m^{-2}, respectively. As a result of the smaller LWP, CNRM-CM5 is slightly closer to LES compared to HadGEM2-A, although there is still not much correlation between the GCM and LES simulated LWP (Figure 7b).

The differences between the LES and the GCM should be interpreted with caution. One caveat is that the LES is forced by long-time mean forcing, while in the GCM the large-scale forcing varies with time. Using time-varying forcing in the LES is computationally expensive as it requires much longer simulations to achieve steady states. For a more systematic comparison with the LES data presented in this paper, one should use a single column model with the same parameterizations as in the GCM and with the same time-mean forcing used to drive the LES. Nevertheless, the fact that the LES forced by large-scale forcings from the two GCMs agree with each other while the GCMs simulate very different clouds still suggest biases in the GCM parameterizations.

3.3 Low cloud response to climate change

One advantage of the forcing framework is that it can be applied to generate LES of changed climates. While previous studies have used LES to simulate cloud responses to idealized climate perturbations (e.g. Blossey et al., 2013; Bretherton et al., 2013; Blossey et al., 2016; Tan et al., 2017; Radtke et al., 2021), driving LES with a GCM allows more realistic representation of changes in large-scale forcings. In this study, we run a set of simulations with large-scale forcings from the AMIP4K experiment, where SST is uniformly increased by 4 K.

Figure 10 shows the change in large-scale forcings and cloud properties in the control and warmer climates at site 17 and site 23 in July in LES driven by HadGEM2-A. At site 17, the large-scale subsidence in the free troposphere is about 20%, or 5% K^{-1}, weaker in the warmer climate. The horizontal advective cooling weakens in the subcloud layer and near the top of the cloud, but strengthens in the lower part of the cloud layer; the change in the advective drying is small. Consistent with weakened subsidence, the cloud top rises slightly in the warmer climate. The cloud base rises more than the cloud top, resulting in a slight thinning of the stratocumulus layer and a decrease in LWP by 13%. The thinning of the cloud layer is likely related to the deepened specific humidity jump at the inversion under warming, which results in more efficient entrainment drying at the cloud top (e.g. Bretherton et al., 2013; Bretherton & Blossey, 2014). At site 23, the weakening of the large-scale subsidence is not uniform with height. Above the cloud top, the subsidence weakens by about 8%, or 2% K^{-1}. The change in the advec-

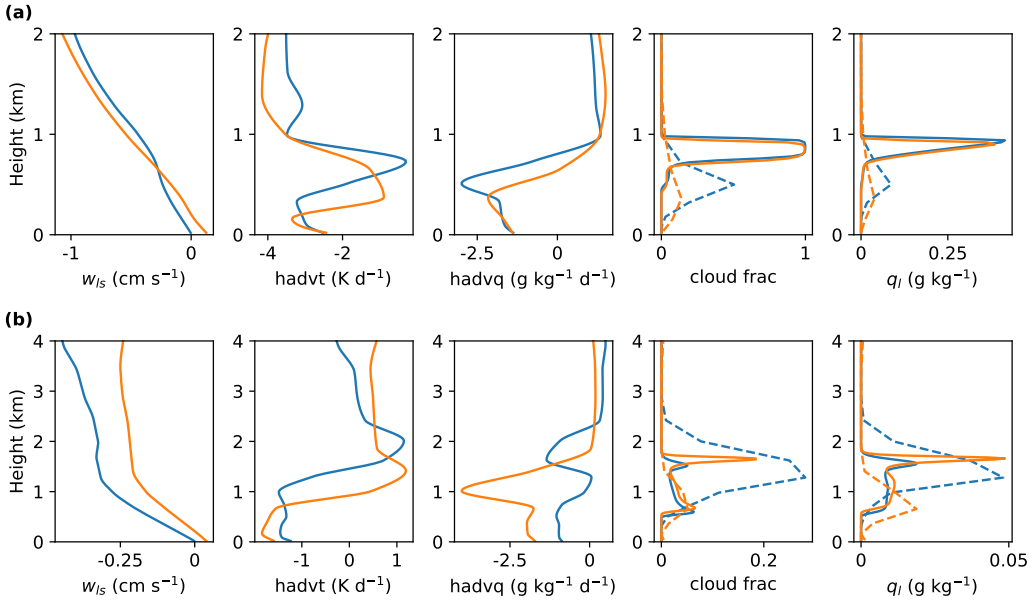

Figure 8: Vertical profiles of large-scale vertical velocity, horizontal advection of temperature, horizontal advection of specific humidity, cloud fraction, and cloud liquid water specific humidity for (a) site 17 and (b) site 23 in July. Blue and orange lines represent LES driven by the large-scale forcing from HadGEM2-A and CNRM-CM5, respectively. Dashed lines represent the host GCMs.

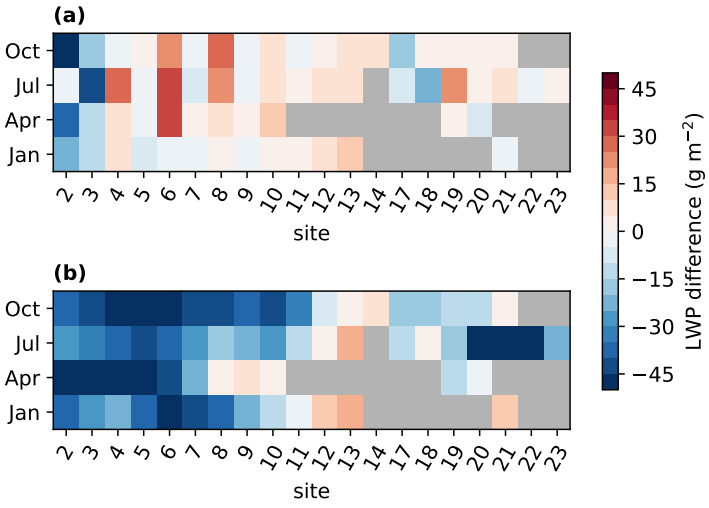

Figure 9: LWP differences at different sites between (a) LES driven by large-scale forcing from HadGEM2-A and CNRM-CM5 and (b) HadGEM2-A and CNRM-CM5. The differences are shown as CNRM-CM5 minus HadGEM2-A. Gray colors indicate the cloud top in at least one of the LES simulations is higher than 3000 m. In the GCMs, LWP is calculated as the vertical integral of cloud liquid water from the surface to 3000 m.

tive tendency of temperature in the boundary layer is small, while the magnitude of the horizontal advective drying increases in the subcloud layer and near the cloud top. Overall the shallow cumulus layer does not change much under warming. There is a slight decrease in cloud fraction near the cloud base. The cloud top rises slightly, and there is an increase in the anvil cloud fraction and cloud liquid water. However, given the large variability in the anvil cloud fraction in the control climate, the change may not be statistically significant.

Figure 11 shows the changes in cloud properties at all sites in different seasons. Near the coasts, the changes in cloud cover and LWP in response to warming are sometimes large, which is usually associated with a change in cloud regimes. However, in shallow cumulus regions, cloud cover and LWP generally do not change or decrease slightly under warming, leading to a small positive shortwave cloud feedback (a small decrease in the magnitude of the shortwave cloud radiative effect). The LES forced by CNRM-CM5 in general also simulate slightly weaker shortwave cloud radiative effects under warming (Figure 12). The magnitude of the cloud response is stronger at several sites in the shallow cumulus regions, which is mostly due to the change in the anvil cloud fraction and cloud liquid water.

Figure 13 compares the LES- and GCM-simulated shortwave cloud feedback averaged over all seasons for the two GCMs. The shortwave cloud feedback is mostly positive in both the LES and the GCM, except at a few sites in CNRM-CM5. While near the coast the feedback magnitude can be as large as 6 W m^{-2} K^{-1} in the LES driven by HadGEM2-A, over the shallow cumulus regions the magnitude is generally smaller than 1 W m^{-2} K^{-1}. This is consistent with estimates of shallow cumulus feedback in previous LES studies (Bretherton, 2015; Nuijens & Siebesma, 2019) and with observationally constrained low cloud feedbacks in recent studies (Cesana & Del Genio, 2021; Myers et al., 2021). However, the shallow cumulus feedback in HadGEM2-A is around 2–4 W m^{-2} K^{-1}, much stronger than that in the LES. In CNRM-CM5, the shortwave cloud feedback is weaker and closer to that in the LES (Figure 13b).

We emphasize again that the difference in the cloud feedback between the LES and GCM should be interpreted with caution. Besides the difference in time-mean and time-varying large-scale forcings as mentioned in Section 3.2, the shortwave cloud feedback in the GCM includes contributions from mid-level and high-level clouds, which are not present in the LES. The difference may also be smaller for other GCMs, as the low-cloud feedback in HadGEM2-A is stronger than in most other GCMs. The climate change simulations provide not only an opportunity to investigate mechanisms governing cloud feedbacks in LES under more realistic changes in large-scale forcings. They are also a valuable dataset for evaluating and calibrating GCM parameterizations, as previous studies have shown it is difficult to guarantee that data-driven parameterizations trained on the current climate remain accurate in a warmer climate (O'Gorman & Dwyer, 2018).

4 Conclusions and Discussion

In this study, we have generated a library of LES spanning a range of low-cloud regimes at multiple locations over the East Pacific, by driving LES with large-scale forcings from CMIP5 GCMs. The LES can simulate the transition from stratocumulus off the coasts to shallow cumulus away from the coasts. The LES results are not very sensitive to the host GCM used to derive the forcings; the differences between clouds simulated by LES driven by different host GCMs are much smaller than the differences between the GCM-simulated clouds. The mismatch between the LES and GCMs may suggest biases in GCM turbulence, convection, and cloud parameterizations. We also used the GCM-driven LES to simulate clouds under climate change with a 4 K increase in SST. In the LES, there is generally a small decrease in cloud cover and LWP in the warmer climate, which results in a weak positive shortwave cloud feedback.

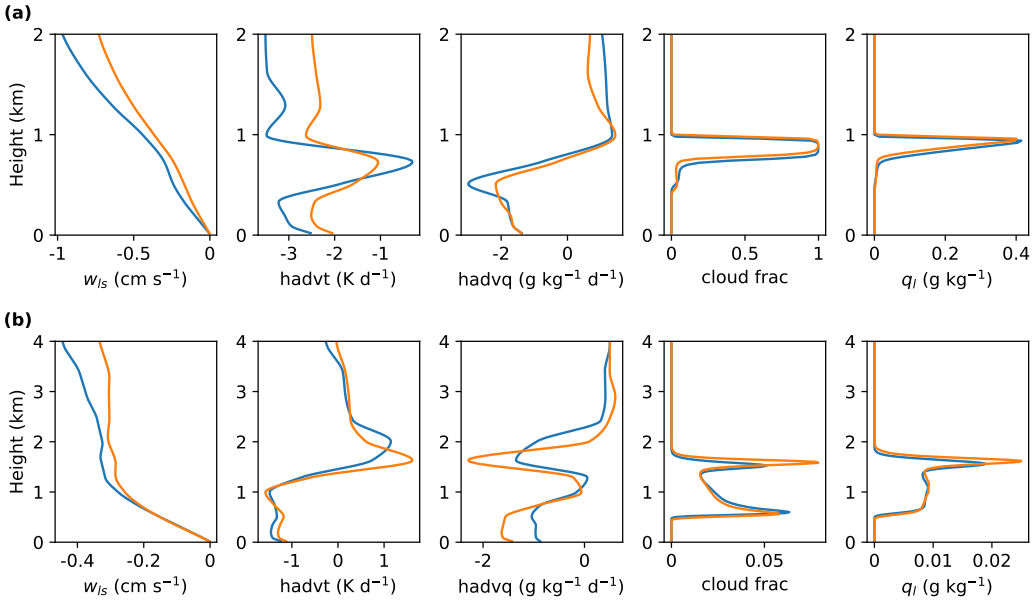

Figure 10: Vertical profiles of large-scale vertical velocity, horizontal advection of temperature, horizontal advection of specific humidity, cloud fraction, and cloud liquid water specific humidity for (a) site 17 and (b) site 23 in July. Blue and orange lines represent LES driven by the large-scale forcing from the AMIP and AMIP4K experiments in HadGEM2-A, respectively.

The LES library, including LES of changed climates, provides an opportunity to systematically train GCM parameterizations. Although the LES may not correctly reproduce clouds in response to time-varying large-scale forcings, the objective is to expand the dataset available for calibrating single column models. To this end, the LES results should be compared with single-column models driven by the same time-mean large-scale forcings, and ideally with the same parameterizations for other physical processes such as radiation and microphysics. The convective parameterization schemes can be calibrated by minimizing mismatches between the LES and single-column models, for example, with Bayesian methods (Cleary et al., 2021). The experimental design allows an iterative workflow, where GCM parameterizations can learn from LES results, and LES can be run with new large-scale forcings from the GCM with improved parameterizations. While this study focused on low clouds over the East Pacific, driving LES with large-scale forcings from GCMs can be done anywhere on the globe. Optimal experimental design approaches can be used to select the locations to generate LES that are most informative about parameterizations (Schneider, Lan, et al., 2017).

The LES of changed climates can also be used to investigate mechanisms of cloud feedbacks under realistic changes in large-scale forcings. This will be explored in more detail in future work.

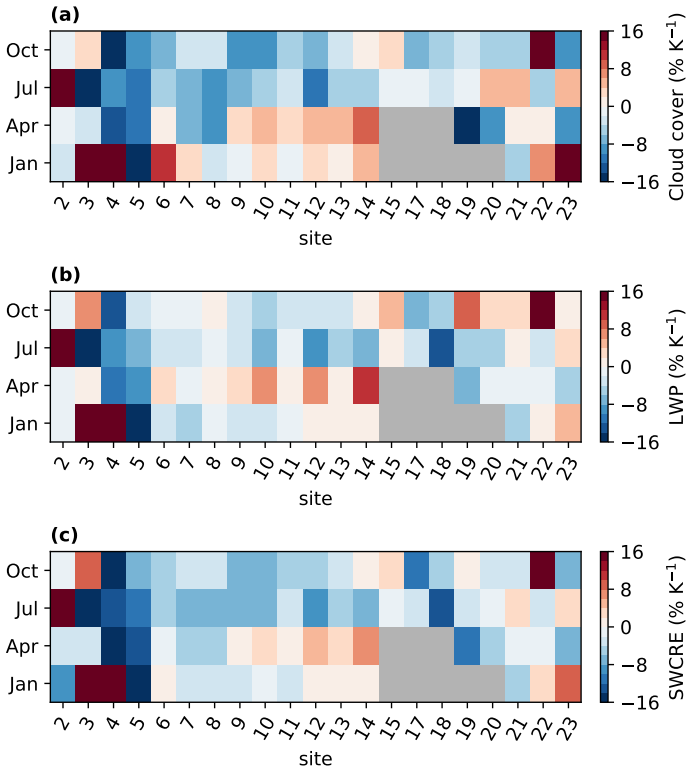

Figure 11: Percentage changes in (a) cloud cover, (b) LWP, and (c) shortwave cloud radiative effect resulting from a 4K increase in SST in the LES driven by HadGEM2-A. Gray colors indicate the cloud top in the LES in the current or warmer climate is higher than 3000 m.

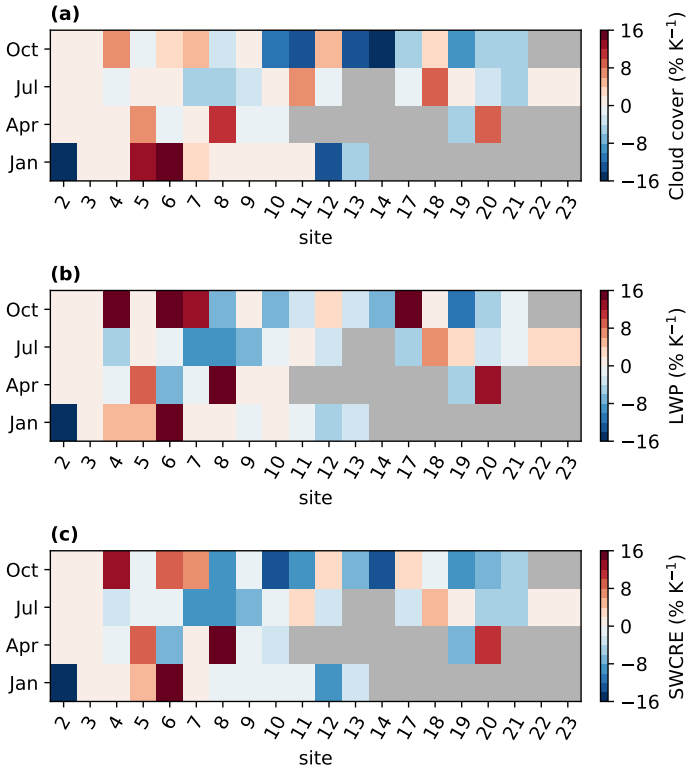

Figure 12: Same as Figure 11 but for LES driven by CNRM-CM5.

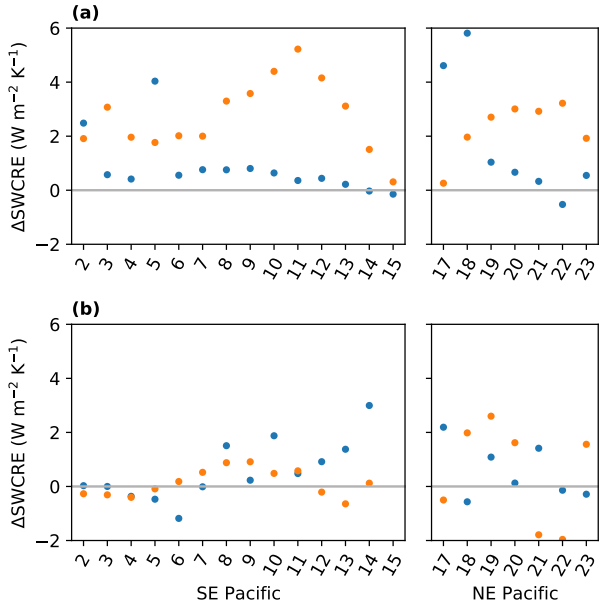

Figure 13: LES (blue) and GCM (orange) simulated shortwave cloud feedback under a 4 K increase in SST. The host GCMs are (a) HadGEM2-A and (b) CNRM-CM5. The results are averaged over all seasons.

Acknowledgments

We thank Yassine Tissaoui and Simone Marras for helpful discussion. We gratefully acknowledge the generous support of Eric and Wendy Schmidt (by recommendation of Schmidt Futures), Charles Trimble, the Paul G. Allen Family Foundation, and the National Science Foundation (Grant 1835860). The simulations were performed on Caltech's High Performance Cluster, which is partially supported by a grant from the Gordon and Betty Moore Foundation. Part of this research was carried out at the Jet Propulsion Laboratory, California Institute of Technology, under a contract with the National Aeronautics and Space Administration. CMIP5 data can be accessed at `https://esgf-node.llnl.gov/projects/cmip5/`. The LES codes are available on the GitHub repository `https://github.com/szy21/pycles_GCM/releases/tag/v1.0`. The LES library will be made publicly available upon acceptance of this paper.

References

Blossey, P. N., Bretherton, C. S., Cheng, A., Endo, S., Heus, T., Lock, A. P., & van der Dussen, J. J. (2016). Cgils p hase 2 les intercomparison of response of subtropical marine low cloud regimes to co 2 quadrupling and a cmip 3 composite forcing change. *Journal of Advances in Modeling Earth Systems*, *8*(4), 1714–1726.

Blossey, P. N., Bretherton, C. S., Zhang, M., Cheng, A., Endo, S., Heus, T., ... Xu, K.-M. (2013). Marine low cloud sensitivity to an idealized climate change: The cgils les intercomparison. *Journal of Advances in Modeling Earth Systems*, *5*(2), 234–258.

Bony, S., Colman, R., Kattsov, V. M., Allan, R. P., Bretherton, C. S., Dufresne, J.-L., ... others (2006). How well do we understand and evaluate climate change feedback processes? *Journal of Climate*, *19*(15), 3445–3482.

Bony, S., & Dufresne, J.-L. (2005). Marine boundary layer clouds at the heart of tropical cloud feedback uncertainties in climate models. *Geophysical Research Letters*, *32*(20).

Bony, S., Webb, M., Bretherton, C., Klein, S., Siebesma, P., Tselioudis, G., & Zhang, M. (2011). Cfmip: Towards a better evaluation and understanding of clouds and cloud feedbacks in cmip5 models.

Bretherton, C. S. (2015). Insights into low-latitude cloud feedbacks from high-resolution models. *Philosophical Transactions of the Royal Society A: Mathematical, Physical and Engineering Sciences*, *373*(2054), 20140415.

Bretherton, C. S., & Blossey, P. N. (2014). Low cloud reduction in a greenhouse-warmed climate: Results from lagrangian les of a subtropical marine cloudiness transition. *Journal of Advances in Modeling Earth Systems*, *6*(1), 91–114.

Bretherton, C. S., Blossey, P. N., & Jones, C. R. (2013). Mechanisms of marine low cloud sensitivity to idealized climate perturbations: A single-les exploration extending the cgils cases. *Journal of Advances in Modeling Earth Systems*, *5*(2), 316–337.

Brient, F., Roehrig, R., & Voldoire, A. (2019). Evaluating marine stratocumulus clouds in the cnrm-cm6-1 model using short-term hindcasts. *Journal of Advances in Modeling Earth Systems*, *11*(1), 127–148.

Brient, F., & Schneider, T. (2016). Constraints on climate sensitivity from space-based measurements of low-cloud reflection. *Journal of Climate*, *29*(16), 5821–5835.

Byun, D. W. (1990). On the analytical solutions of flux-profile relationships for the atmospheric surface layer. *Journal of Applied Meteorology (1988-2005)*, 652–657.

Cesana, G., & Del Genio, A. D. (2021). Observational constraint on cloud feedbacks suggests moderate climate sensitivity. *Nature Climate Change*, *11*(3), 213–218.

Cesana, G., & Waliser, D. (2016). Characterizing and understanding systematic biases in the vertical structure of clouds in cmip5/cfmip2 models. *Geophysical Research Letters*, *43*(19), 10–538.

Cleary, E., Garbuno-Inigo, A., Lan, S., Schneider, T., & Stuart, A. M. (2021). Calibrate, emulate, sample. *Journal of Computational Physics*, *424*, 109716.

Iacono, M. J., Delamere, J. S., Mlawer, E. J., Shephard, M. W., Clough, S. A., & Collins, W. D. (2008). Radiative forcing by long-lived greenhouse gases: Calculations with the aer radiative transfer models. *Journal of Geophysical Research: Atmospheres*, *113*(D13).

Kessler, E. (1995). On the continuity and distribution of water substance in atmospheric circulations. *Atmospheric research*, *38*(1-4), 109–145.

Klein, S. A., Zhang, Y., Zelinka, M. D., Pincus, R., Boyle, J., & Gleckler, P. J. (2013). Are climate model simulations of clouds improving? an evaluation using the isccp simulator. *Journal of Geophysical Research: Atmospheres*, *118*(3), 1329–1342.

Lilly, D. K. (1962). On the numerical simulation of buoyant convection. *Tellus*, *14*(2), 148–172.

Myers, T. A., Scott, R. C., Zelinka, M. D., Klein, S. A., Norris, J. R., & Caldwell, P. M. (2021). Observational constraints on low cloud feedback reduce uncertainty of climate sensitivity. *Nature Climate Change*, 1–7.

Nam, C., Bony, S., Dufresne, J.-L., & Chepfer, H. (2012). The 'too few, too bright'tropical low-cloud problem in cmip5 models. *Geophysical Research Letters*, *39*(21).

Neggers, R. A., Siebesma, A., & Heus, T. (2012). Continuous single-column model evaluation at a permanent meteorological supersite. *Bulletin of the American Meteorological Society*, *93*(9), 1389–1400.

Nuijens, L., & Siebesma, A. P. (2019). Boundary layer clouds and convection over subtropical oceans in our current and in a warmer climate. *Current Climate Change Reports*, *5*(2), 80–94.

O'Gorman, P. A., & Dwyer, J. G. (2018). Using machine learning to parameterize moist convection: Potential for modeling of climate, climate change, and extreme events. *Journal of Advances in Modeling Earth Systems*, *10*(10), 2548–2563.

Pressel, K. G., Kaul, C. M., Schneider, T., Tan, Z., & Mishra, S. (2015). Large-eddy simulation in an anelastic framework with closed water and entropy balances. *Journal of Advances in Modeling Earth Systems*, *7*(3), 1425–1456.

Pressel, K. G., Mishra, S., Schneider, T., Kaul, C. M., & Tan, Z. (2017). Numerics and subgrid-scale modeling in large eddy simulations of stratocumulus clouds. *Journal of advances in modeling earth systems*, *9*(2), 1342–1365.

Radtke, J., Mauritsen, T., & Hohenegger, C. (2021). Shallow cumulus cloud feedback in large eddy simulations–bridging the gap to storm-resolving models. *Atmospheric Chemistry and Physics*, *21*(5), 3275–3288.

Randall, D. A., & Cripe, D. G. (1999). Alternative methods for specification of observed forcing in single-column models and cloud system models. *Journal of Geophysical Research: Atmospheres*, *104*(D20), 24527–24545.

Rauber, R. M., Stevens, B., Ochs III, H. T., Knight, C., Albrecht, B., Blyth, A., ... others (2007). Rain in shallow cumulus over the ocean: The rico campaign. *Bulletin of the American Meteorological Society*, *88*(12), 1912–1928.

Schneider, T., Lan, S., Stuart, A., & Teixeira, J. (2017). Earth system modeling 2.0: A blueprint for models that learn from observations and targeted high-resolution simulations. *Geophysical Research Letters*, *44*(24), 12–396.

Schneider, T., Teixeira, J., Bretherton, C. S., Brient, F., Pressel, K. G., Schär, C., & Siebesma, A. P. (2017). Climate goals and computing the future of clouds. *Nature Climate Change*, *7*(1), 3–5.

Shen, Z., Pressel, K. G., Tan, Z., & Schneider, T. (2020). Statistically steady state

large-eddy simulations forced by an idealized gcm: 1. forcing framework and simulation characteristics. *Journal of Advances in Modeling Earth Systems*, *12*(2), e2019MS001814.

Shu, C.-W., & Osher, S. (1988). Efficient implementation of essentially non-oscillatory shock-capturing schemes. *Journal of computational physics*, *77*(2), 439–471.

Siebesma, A. P., Bretherton, C. S., Brown, A., Chlond, A., Cuxart, J., Duynkerke, P. G., ... others (2003). A large eddy simulation intercomparison study of shallow cumulus convection. *Journal of the Atmospheric Sciences*, *60*(10), 1201–1219.

Smagorinsky, J. (1963). General circulation experiments with the primitive equations: I. the basic experiment. *Monthly weather review*, *91*(3), 99–164.

Stevens, B., Moeng, C.-H., Ackerman, A. S., Bretherton, C. S., Chlond, A., de Roode, S., ... others (2005). Evaluation of large-eddy simulations via observations of nocturnal marine stratocumulus. *Monthly weather review*, *133*(6), 1443–1462.

Tan, Z., Schneider, T., Teixeira, J., & Pressel, K. G. (2016). Large-eddy simulation of subtropical cloud-topped boundary layers: 1. a forcing framework with closed surface energy balance. *Journal of Advances in Modeling Earth Systems*, *8*(4), 1565–1585.

Tan, Z., Schneider, T., Teixeira, J., & Pressel, K. G. (2017). Large-eddy simulation of subtropical cloud-topped boundary layers: 2. cloud response to climate change. *Journal of Advances in Modeling Earth Systems*, *9*(1), 19–38.

Vignesh, P. P., Jiang, J. H., Kishore, P., Su, H., Smay, T., Brighton, N., & Velicogna, I. (2020). Assessment of cmip6 cloud fraction and comparison with satellite observations. *Earth and Space Science*, *7*(2), e2019EA000975.

Zelinka, M. D., Myers, T. A., McCoy, D. T., Po-Chedley, S., Caldwell, P. M., Ceppi, P., ... Taylor, K. E. (2020). Causes of higher climate sensitivity in cmip6 models. *Geophysical Research Letters*, *47*(1), e2019GL085782.

Zhang, M., Bretherton, C. S., Blossey, P. N., Austin, P. H., Bacmeister, J. T., Bony, S., ... others (2013). Cgils: Results from the first phase of an international project to understand the physical mechanisms of low cloud feedbacks in single column models. *Journal of Advances in Modeling Earth Systems*, *5*(4), 826–842.

Zhang, M., Bretherton, C. S., Blossey, P. N., Bony, S., Brient, F., & Golaz, J.-C. (2012). The cgils experimental design to investigate low cloud feedbacks in general circulation models by using single-column and large-eddy simulation models. *Journal of Advances in Modeling Earth Systems*, *4*(4).